Composites: Part A 94 (2017) 41–49

Contents lists available at ScienceDirect

Composites: Part A

journal homepage: www.elsevier.com/locate/compositesa

N-doped reduced graphene oxide/waterborne polyurethane composites prepared by in situ chemical reduction of graphene oxide

Konghu Tian [a,b], Zheng Su [a,b], Hua Wang [a,*], Xingyou Tian [a,**], Weiqi Huang [a,b], Chao Xiao [a,b]

[a] Institute of Applied Technology, Hefei Institutes of Physical Science, Chinese Academy of Sciences, Hefei 230031, PR China
[b] University of Science and Technology of China, Hefei 230026, PR China

ARTICLE INFO

Article history:
Received 1 September 2016
Received in revised form 17 November 2016
Accepted 17 November 2016
Available online 18 November 2016

Keywords:
A. Polymer-matrix composites (PMCs)
A. Graphene
E. Assembly

ABSTRACT

In this study, N-doped reduced graphene oxide/waterborne polyurethane (NRGO/WPU) composites were prepared by in situ chemical reduction of graphene oxide in an aqueous solution system. The morphology, structure, electrical conductivity, electromagnetic shielding, as well as thermal stability of the NRGO/WPU composites were characterized. The results show that simultaneous chemical reduction and N-doped functionalization of graphene oxide were achieved using diethylenetriamine as a reducing agent and N-doping agent. The introduction of NRGO could endow the WPU with quality electromagnetic interference shielding effectiveness (EMI SE). The composites with 12 wt% NRGO content exhibited the EMI SE of 28.3 dB at 9 GHz. Attributable to the uniform distribution of NRGO in the WPU matrix and its formed network structure, the NRGO/WPU composites had a better electrical conductivity compared with virgin WPU. TG and DTG indicated that the NRGO/WPU composites had a better thermal stability than virgin WPU.

1. Introduction

Graphene, a new kind of carbon material possessing two-dimensional layers with a honeycomb lattice, has drawn great attentions due to its unique physical and chemical properties [1–4]. In order to meet the application needs of the future semiconductor device and electronics industry, many research works were focused on the preparation methods and performance analysis of graphene and its functional derivatives [5–8]. Among these, N-doped reduced graphene oxide (NRGO) was considered an ideal and effective route to modulate and control the properties of graphene for applications [9–12].

Graphene/polymer composites synergistically combined the properties of the host polymer matrix and discrete graphene, thus their physicochemical characteristics significantly differed from those of the bulk materials. These composite materials were expected to have novel electrical [13–15], optical [16,17], thermal [18–20], mechanical [21–23], microwave absorption [24], and electromagnetic interference shield [25,26] properties. Therefore, graphene was considered an exemplary nanofiller to improve properties of polymer composites. Graphene/polymer composites were mostly obtained via the mixing of graphene with polymer. However, to form composites with predetermined excellent performances, many challenges and difficulties were involved, such as improving interfacial adhesion between graphene and the polymer matrix, and preventing graphene from aggregation in the polymer matrix [27,28]. To maintain a uniform and stable dispersion of graphene in the polymer matrix, several experimentations focused on the method of in situ chemical reduction of graphene oxide in an aqueous media with waterborne polymer [29–31]. To the best of our knowledge, this method could be used for the preparation of N-doped reduced graphene oxide/waterborne polyurethane (NRGO/WPU) composites.

Recently, some scientific papers have been published regarding the preparation and characterization of reduced graphene oxide/water-borne polyurethane (RGO/WPU) composites. Hsiao et al. prepared RGO/WPU composites through the electrospinning and layer-by-layer assembly technique, with the obtained composites exhibiting good electrical conductivity and EMI shielding effectiveness [32]. Yousefi et al. used hydrazine solution as a reducing agent to obtain RGO/WPU composites, and the composites showed substantially enhanced tensile strength, as well as a systematic reduction of the moisture permeability with increasing RGO content [33]. Lei et al. used 3-aminopropyltriethoxysilane as a modifying agent and diethanol amine as a reducing agent to obtain RGO/WPU composites, the composites' film expressed better thermal

* Corresponding author.
** Corresponding author.
E-mail addresses: wanghua@issp.ac.cn (H. Wang), xytian@issp.ac.cn (X. Tian).

http://dx.doi.org/10.1016/j.compositesa.2016.11.020
1359-835X/

stability than that of virgin WPU [34]. In this article, NRGO/WPU composites were prepared by in situ chemical reduction of graphene oxide in an aqueous solution system. It is worth mentioning that the preparation process, without complicated procedure and equipment, was a facile and effective method to prepare NRGO/WPU composites. Not only was simultaneous chemical reduction and N-doped functionalization of graphene oxide realized when diethylenetriamine was used as a reducing agent and N-doping agent, but the uniform distribution of NRGO in the WPU matrix was also achieved. The electrical conductivity, electromagnetic shielding, and thermal stability of NRGO/WPU composites were all studied in detail.

2. Experimental

2.1. Material

The natural graphite powder was purchased from Qingdao Huatai Lubricant Sealing S&T Co., Ltd. The aqueous emulsion of WPU (PU-2960) was supplied by ShunDe SanSheng Trade Co., Ltd. Concentrated sulfuric acid (analytical reagent, 95–98 wt%), potassium permanganate (analytical reagent) and hydrochloric acid (analytical reagent, 36–38 wt%) were purchased from Sinopharm Chemical Reagent Co., Ltd. Sodium nitrate (analytical reagent), H_2O_2 (analytical reagent, 30 wt%) and diethylenetriamine (DETA, analytical reagent) were purchased from Shanghai Aladdin Bio-Chem Technology Co., Ltd.

2.2. Preparation of GO

GO was synthesized based on natural graphite using the modified Hummers chemical method [35,36]. Natural graphite (2.5 g) and sodium nitrate (1.9 g) were added to concentrated sulfuric acid (200 ml) in a round-bottom flask. The flask was put into an ice bath to keep the temperature of the mixture less than 5 °C. Under stirring with a speed of 150 rpm, potassium permanganate (7.5 g) was slowly added to the reaction mixture. After that, the temperature of the reaction mixture was heated up to 35 °C and stirred for 48 h. Deionized water (150 ml) was subsequently added to the reaction mixture. Then the temperature was heated up to 90 °C and stirred for 3 h. H_2O_2 (40 ml) was added to the reaction mixture after the temperature below 30 °C. The reaction mixture was centrifuged and washed with an aqueous solution of hydrochloric acid (5 wt%) and deionized water for four times. Finally, the GO dispersion was centrifuged at 3000 rpm for 20 min to remove the unexfoliated graphite.

2.3. Preparation of NRGO

For the flask containing the GO dispersion above, 10 wt% DETA was added under stirring with a speed of 150 rpm. The reaction mixture was kept at 80 °C for 24 h to obtain NRGO dispersion. Then, NRGO was obtained by centrifugation, washing, and drying.

2.4. Preparation of NRGO/WPU composites

The GO dispersion was added to the flask containing WPU emulsion in an ultrasonic bath. Then, 10 wt% DETA was added to the mixture under stirring with a speed of 150 rpm. The reaction mixture was kept at 80 °C for 24 h to obtain NRGO/WPU composites dispersion. The NRGO/WPU composites dispersion was transferred into a Teflon molds and dried at 50 °C for 24 h in a vacuum dry oven, the composites sample was obtained as a result. Then, the sample was washed with DI water and acetone at 40 °C for 12 h. The washing procedure described above was repeated for three times. Finally, the composites samples were obtained by vacuum drying at 70 °C for 24 h.

2.5. Characterization

Fourier transform infrared spectra (FTIR) of the samples were recorded on a Nicolet 8700 spectrometer. Raman spectra of the samples were recorded using a Renishaw in Via Reflex Raman system with an excitation laser of 532 nm. X-ray diffraction (XRD) patterns of the samples were performed in the range of $2\theta = 5–80°$ by a Philips X'Pert Pro MPD X-ray diffractometer, using Cu Kα radiation ($\lambda = 0.15406$ nm). The transmission emission microscopy (TEM) of the samples were observed on a JEM-2010 TEM. Zeta potential of the samples were measured using a Malvern 3000HSA zetasizer instrument. The scanning electron microscopy (SEM) of the samples were observed on a Sirion-200 field emission scanning electron microscope with an accelerating voltage of 20 kV. The LK2679A high resistivity meter was used to measure the electrical conductivity of samples with volume resistivity beyond 10^6 Ω cm at room temperature. The RTS-9 four-point probe resistivity measurement system was used to measure the electrical conductivity of samples with volume resistivity within 10^6 Ω cm at room temperature. The electromagnetic interference (EMI) shielding effectiveness of the samples were obtained using a AV3629A vector network analyzer, the toroidal shaped samples with an outer diameter of 7.0 mm and inner diameter of 3.0 mm, a frequency range of 1–9 GHz. The thermal gravimetric (TG) and differential thermal gravimetric (DTG) analysis of the samples were tested by a Q5000 IR thermal gravimetric analyzer at a heating rate of 10 °C/min in air atmosphere. XPS spectra of the samples were obtained via an X-ray photoelectron spectroscopy (American Thermo).

3. Results and discussions

3.1. Chemical and morphology analyses of GO and NRGO

In this study, NRGO was successfully synthesized via a simultaneous chemical reduction and N-doped functionalization of GO. The spectra of GO and NRGO are shown in Fig. 1. In the FTIR spectra of GO and NRGO, the bands of 2923 cm^{-1} and 2850 cm^{-1} were attributed to the stretching vibrations of the C—H bond. For GO,

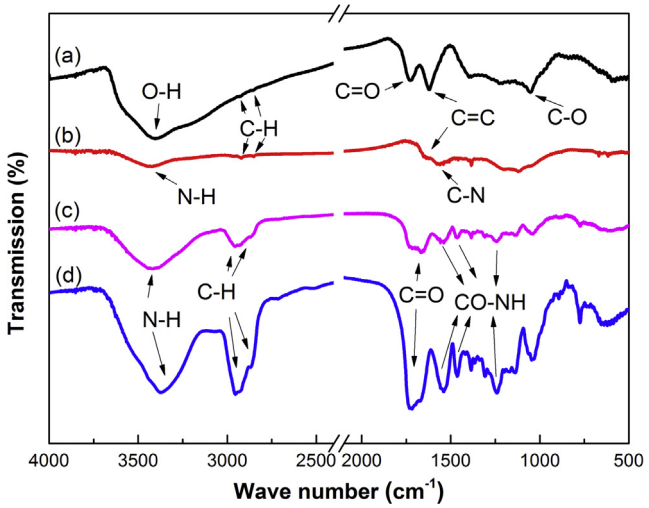

Fig. 1. FTIR spectra of (a) GO, (b) NRGO, (c) NRGO/WPU composites containing 5 wt % NRGO, and (d) WPU. (For interpretation of the references to colour in this figure legend, the reader is referred to the web version of this article.)

the band of 3406 cm^{-1} was attributed to stretching vibrations of the O—H bond. The peak at 1721 cm^{-1} was attributed to the stretching vibrations of the C=O bond of carbonyl or carboxyl groups. The peak at 1622 cm^{-1} corresponded to the stretching vibrations of the C=C bond of the benzene rings of GO. Deformation vibrations of the C—O bond were observed at 1051 cm^{-1} [37]. For NRGO, the band of 3423 cm^{-1} was attributed to the stretching vibrations of the N—H bond. The peaks at 1640 cm^{-1} and 1575 cm^{-1} corresponded to the stretching vibrations of the C=C bond and the C=N bond, respectively. Due to the acylation reaction, the band of C=C bond moved from 1622 cm^{-1} to 1640 cm^{-1} compared with GO [31,38]. The bands of the C=O bond and the C—O bond in the FTIR spectra of NRGO were weakened. This result confirmed the reduction reaction of DETA to GO.

Fig. 2 shows the Raman spectra of GO, NRGO, and natural graphite samples. Raman spectroscopy is a very valuable characterization method for carbon materials. In the Raman spectrum of GO, NRGO, and natural graphite samples, the D band originated from the presence of disordered carbon or defected mode of the carbon lattices' materials. The G band was usually attributed to the in-plane stretching vibrations of sp^2 hybrid mode carbon atom in all of the samples. As shown in Fig. 2, D band and G band were located at about 1340–1350 cm^{-1} and 1580–1590 cm^{-1}, respectively. I_D was the integral area of D band, I_G was the integral area of G band, and the normalized I_D/I_G ratio was used to measure the amount of disorder of samples [39]. According to calculation, the values of I_D/I_G ratio of GO, NRGO and natural graphite were 1.45, 1.13, and 0.08, respectively. Compared to graphite, the higher value of I_D/I_G ratio of GO meant that graphite was effectively exfoliated into GO layers. Compared to GO, the lower value of I_D/I_G ratio of NRGO indicated that reduction of GO led to the improvement of the ordering of NRGO sample [40].

As shown in Fig. 3, XRD patterns were employed to identify the GO, NRGO, and natural graphite. In curve c, the major characteristic diffraction peaks were at $2\theta = 26.6°$, 44.6°, and 54.7°, corresponding to the (0 0 2), (1 0 1), and (0 0 4) crystal faces of graphite (JCPDF No. 00-008-0415) [41]. According to Bragg law, the interplanar spacing of graphite calculated was 3.35 Å. In curve b, the major characteristic diffraction peak was at $2\theta = 10.7°$ of GO, corresponding to the (0 0 1) crystal face of GO [42]. According to Bragg law, the interplanar spacing of GO was 8.25 Å, which indicated that the interplanar spacing of GO had obviously increased compared

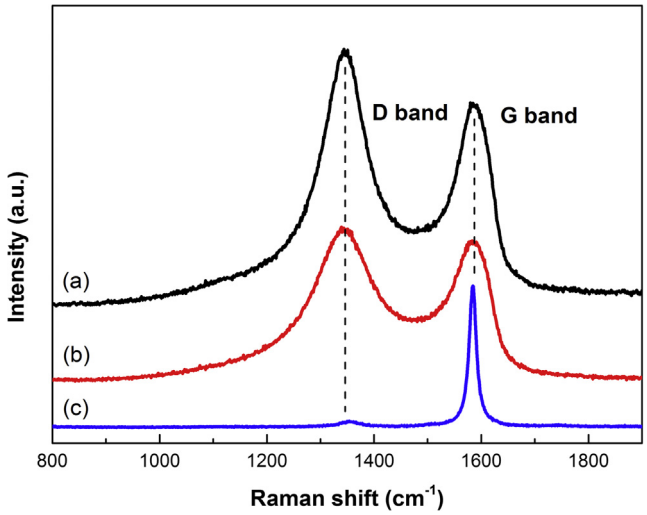

Fig. 2. Raman spectra of (a) GO, (b) NRGO, and (c) natural graphite. (For interpretation of the references to colour in this figure legend, the reader is referred to the web version of this article.)

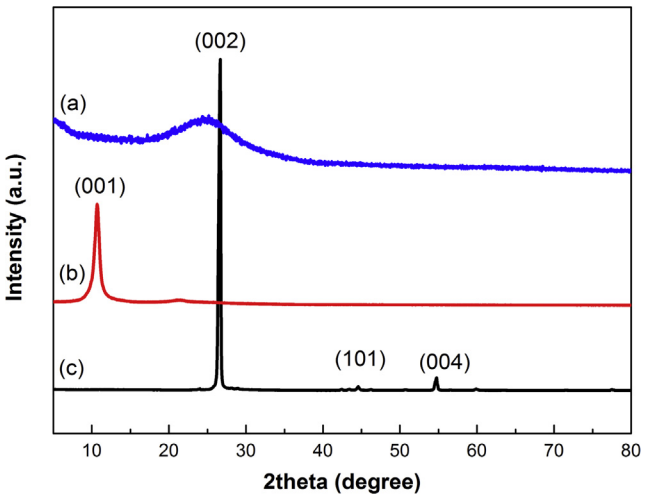

Fig. 3. XRD patterns of (a) NRGO, (b) GO, and (c) natural graphite. (For interpretation of the references to colour in this figure legend, the reader is referred to the web version of this article.)

to graphite. In curve a, there was a board peak at $2\theta = 24.3°$, which indicated that the structure of NRGO was comprised of randomly ordered graphitic platelets [43]. The result confirmed the reduction reaction of DETA to GO.

Fig. 4 shows the TEM images of GO and NRGO. The morphology of GO displays the flat surface, while the obvious wrinkle appears on the surface of NRGO. The morphology change was attributable to the effect of chemical reduction of DETA to GO, which introduced the defects of hexagon–heptagon rings on the surface of NRGO, leading to the wrinkled and fluffy surface [44,45]. After the chemical reduction of DETA, some XPS characteristic peaks of GO, especially for C=O (287.1 eV) (Fig. 4e), were greatly weakened, shifted, or disappeared, which suggested the removal of oxygen-containing groups and then confirmed the efficient reduction of DETA to GO. In Fig. 4f, the additional component at 286.4 eV could be ascribed to C—N groups. Moreover, it should be noted that survey XPS spectra of NRGO (Fig. 4c) showed the apparent nitrogen peak at ~401 eV and decreased oxygen peak at ~530 eV as compared to that of GO, which indicated the de-oxygenation or oxygen substitution by nitrogen [37,46]. This result supported the reduction and N-doped functionalization of GO by DETA.

3.2. Chemical and morphology analyses of NRGO/WPU composites

In this study, NRGO/WPU composites were successfully prepared by the in situ chemical reduction method. The photo images of WPU (10.0 mg/ml), GO (0.5 mg/ml), GO/WPU composites (10.0 mg/ml) and NRGO/WPU composites (10.0 mg/ml) dispersion are shown in Fig. 5. The FTIR spectra of NRGO/WPU composites and WPU are shown in Fig. 1. In the FTIR spectra of NRGO/WPU composites and WPU, the band of 3374 cm^{-1} was ascribed to the stretching vibrations of the N—H bond. The bands of 2954 cm^{-1} and 2855 cm^{-1} were attributed to the stretching vibrations of the C—H bond. The peak at 1721 cm^{-1} was ascribed to the stretching vibrations of the C=O bond of carbonyl or carboxyl groups. Furthermore, the peaks of 1539 cm^{-1}, 1463 cm^{-1}, and 1241 cm^{-1} were attributed to the stretching vibrations of the CO—NH groups [47].

In order to explore the formation mechanism of NRGO/WPU composites, the Zeta potential (ξ) of GO dispersion, WPU dispersion, GO/WPU composites dispersion and NRGO/WPU composites dispersion were measured. The Zeta potential of GO dispersion (0.05 mg/ml) and WPU dispersion (1.0 mg/ml) were −52 mV and

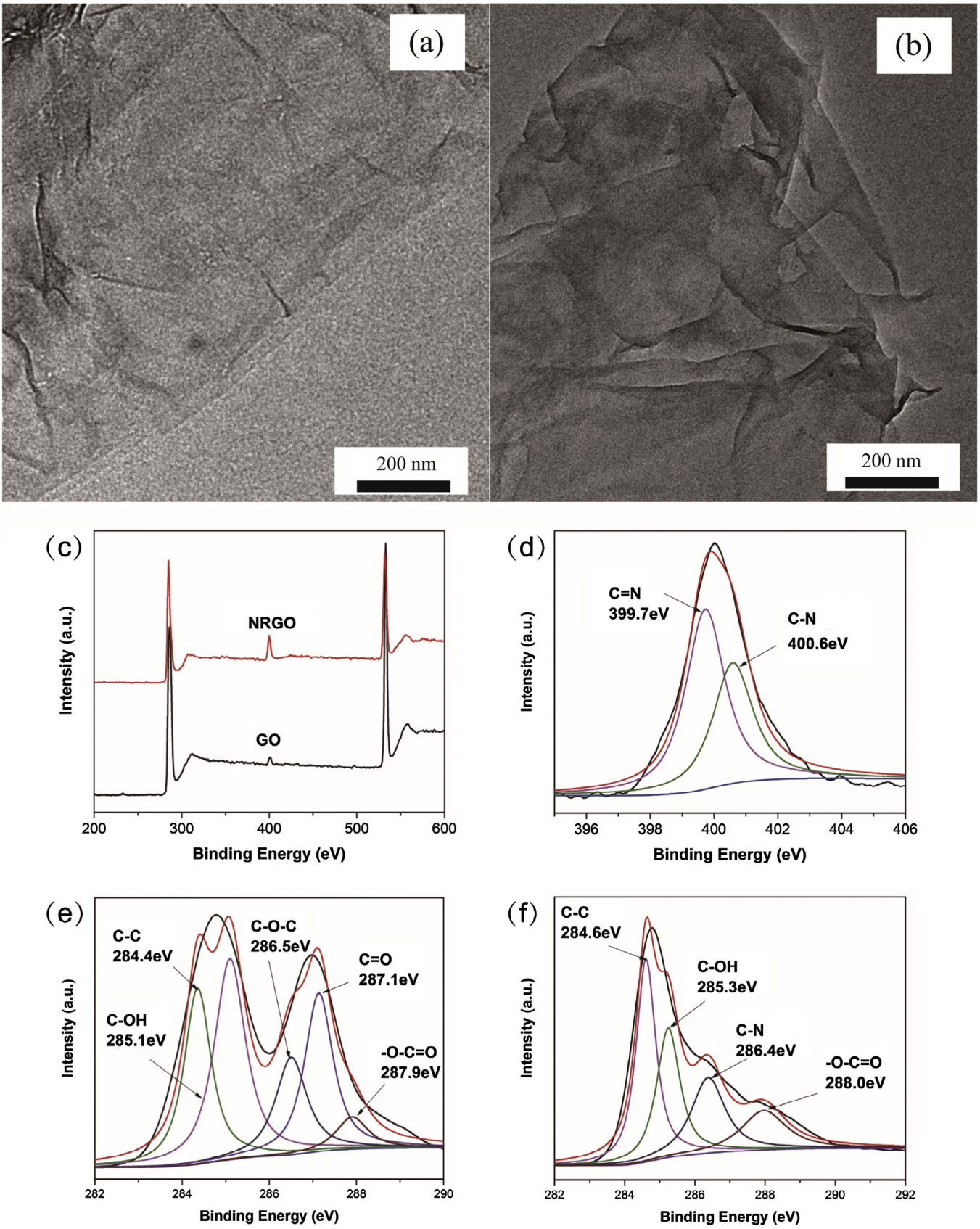

Fig. 4. TEM images of (a) GO, and (b) NRGO; (c) survey XPS spectra of GO and NRGO; (d) N1s spectrum of NRGO; (e) C1s spectrum of GO; (f) C1s spectrum of NRGO. (For interpretation of the references to colour in this figure legend, the reader is referred to the web version of this article.)

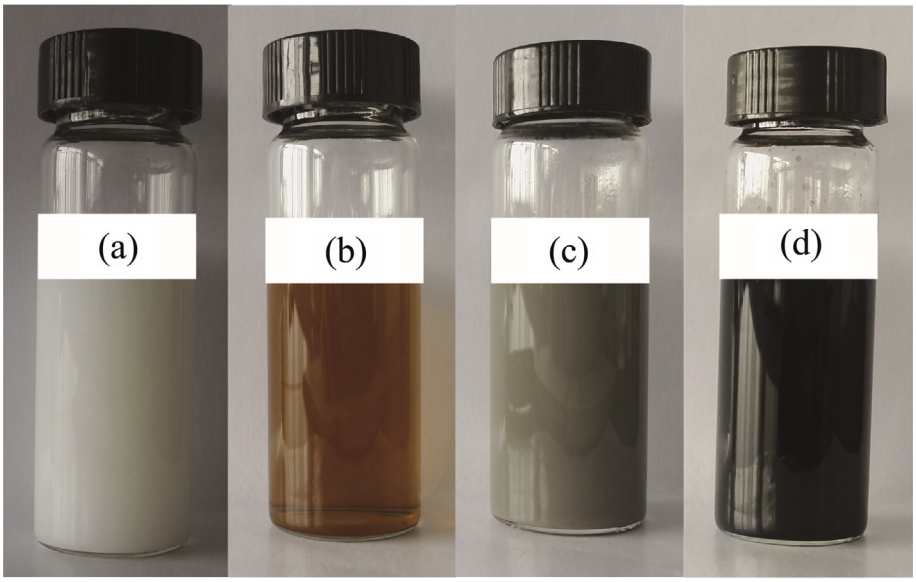

Fig. 5. Photo images of (a) WPU dispersion, (b) GO dispersion, (c) GO/WPU composites dispersion and (d) NRGO/WPU composites dispersion. (For interpretation of the references to colour in this figure legend, the reader is referred to the web version of this article.)

−43 mV, respectively. Although both of them were negatively charged, they could form a stable GO/WPU composites dispersion (1.05 mg/ml) containing 5 wt% GO content ($\xi = -67$ mV). Similar to other recent studies, the polyurethane chains could be self-assembled and adsorbed onto the surface of the GO sheet. The negatively charged or oxygenated groups were hydrophilic, in other words they were mostly located at the edge of GO sheet surface [48–51]. Thereafter, DETA was fed into the dispersion of the GO/WPU composites, the NRGO/WPU composites dispersion containing 5 wt% NRGO content with $\xi = -56$ mV (1.05 mg/ml) was obtained by the in situ chemical reduction method. The formation process of NRGO/WPU composites is shown in Fig. 6.

In order to explore the dispersion of NRGO in the NRGO/WPU composites, SEM images of GO, NRGO, virgin WPU, and NRGO/WPU composites, as well as TEM image of NRGO/WPU composites were measured. The results are shown in Fig. 7. Consistent with the result of TEM, the SEM of GO showed a relatively flat surface (Fig. 7a), while the evident wrinkle appeared on the surface of NRGO (Fig. 7b). The morphology change was attributable to the effect of chemical reduction of DETA to GO, which introduced hexagon–heptagon rings defects on the surface of NRGO, which led to the wrinkled and fluffy surface [44,45]. Fig. 7c shows the SEM image of the virgin WPU. From it, we could see that the virgin WPU matrix had a smooth and flat fractured surface without an obvious wrinkle. Fig. 7d–g displays the SEM images of NRGO/WPU composites with 1.0, 5.0, 9.0 and 12.0 wt% NRGO content, respectively. There existed a rough fractured surface with many wrinkles, which indicated that NRGO had a good dispersion in the composites. Fig. 7h shows the TEM image of NRGO/WPU composites with 5.0 wt% NRGO content. By observing this image, we can see that NRGO formed a continuous network structure in the composites. The uniform distribution of NRGO in the WPU matrix and its formed network structure could be beneficial to improve the electrical conductivity and EMI shielding effectiveness of NRGO/WPU composites.

3.3. Electrical conductivity performance of NRGO/WPU composites

The results of the studied conductivity of NRGO/WPU composites are shown in Fig. 8. When the NRGO content changed from 1 to 12 wt%, the electrical conductivity of NRGO/WPU composites showed a rapid increase at low content, and then slowly climbed

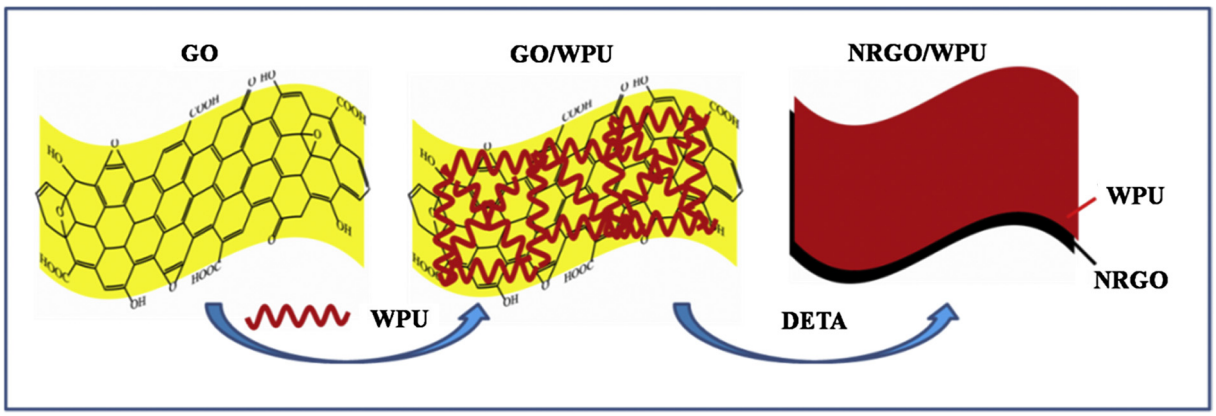

Fig. 6. Schematic illustration of formation mechanism for the NRGO/WPU composites. (For interpretation of the references to colour in this figure legend, the reader is referred to the web version of this article.)

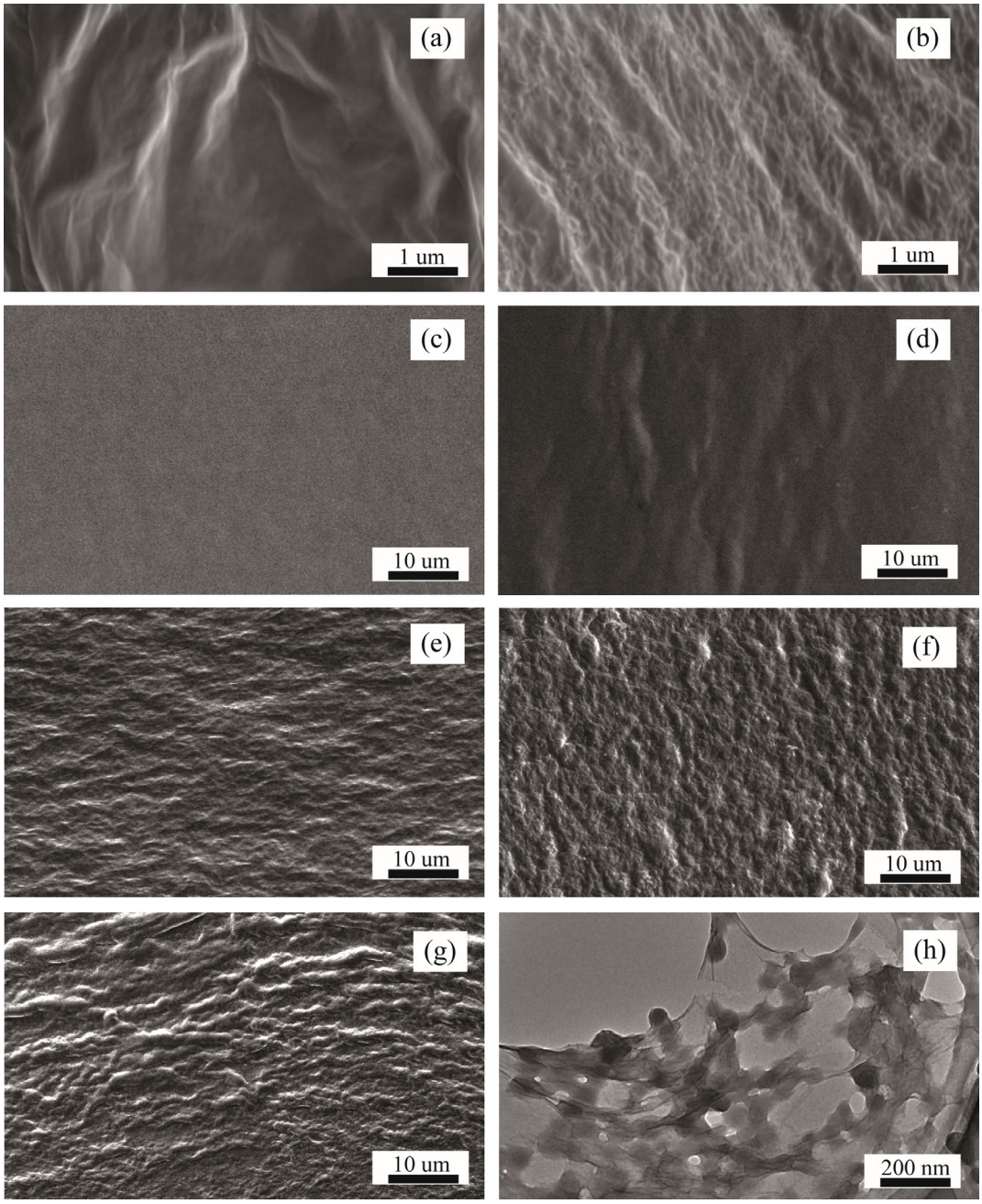

Fig. 7. SEM images of (a) GO, (b) NRGO, (c) virgin WPU, and NRGO/WPU composites containing (d) 1 wt% NRGO, (e) 5 wt% NRGO, (f) 9 wt% NRGO, and (g) 12 wt% NRGO; TEM image of (h) NRGO/WPU composites containing 5 wt% NRGO.

with the increase of NRGO content. Percolation theory defined an insulator-conductor transition and the corresponding threshold concentration of the conductive filler, via the following equation [52,53]:

$$\sigma = \sigma_0(\rho - \rho_c)^t \text{ for } \rho > \rho_c \quad (1)$$

where σ is the conductivity of NRGO/WPU composites, σ_0 is a constant, ρ is the content of NRGO, ρ_c is the percolation threshold content of NRGO, and t is the critical exponent.

According to Eq. (1), $\rho_c = 0.078$ vol%, and $t = 1.98 \pm 0.11$ for NRGO/WPU composites. When the NRGO content exceeded the corresponding threshold content, the NRGO/WPU composites had exceptional electrical conductivity, owing to the network structure of NRGO in the WPU matrix. The best electrical conductivity of composites was 0.08 S/cm with 12 wt% NRGO content. The high electrical conductivity of NRGO/WPU composites and the uniform distribution of NRGO in the WPU matrix could improve the EMI shielding performances of NRGO/WPU composites [54].

3.4. EMI shielding performance of NRGO/WPU composites

We investigated the EMI shielding effectiveness (SE) of NRGO/WPU composites. As shown in Fig. 9, the EMI SE of NRGO/WPU composites exhibited the variation in the frequency range from 1 to 9 GHz with various NRGO contents. On account of the conductivity of NRGO content and its formed network structure, the results show that the EMI SE performances increased with

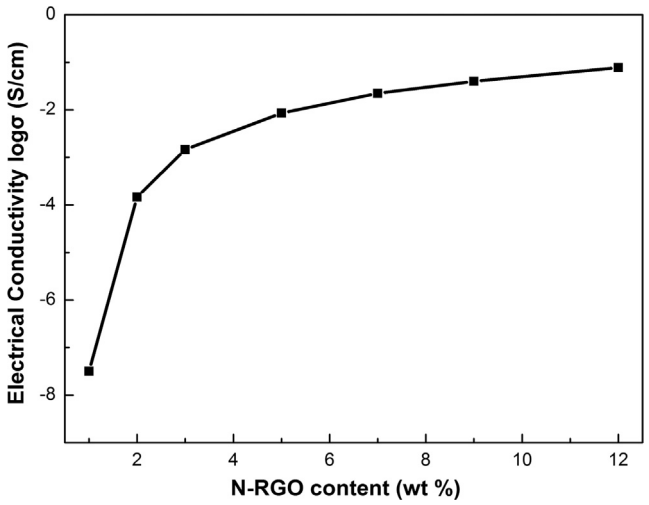

Fig. 8. Electrical conductivity of NRGO/WPU composites with different NRGO content. (For interpretation of the references to colour in this figure legend, the reader is referred to the web version of this article.)

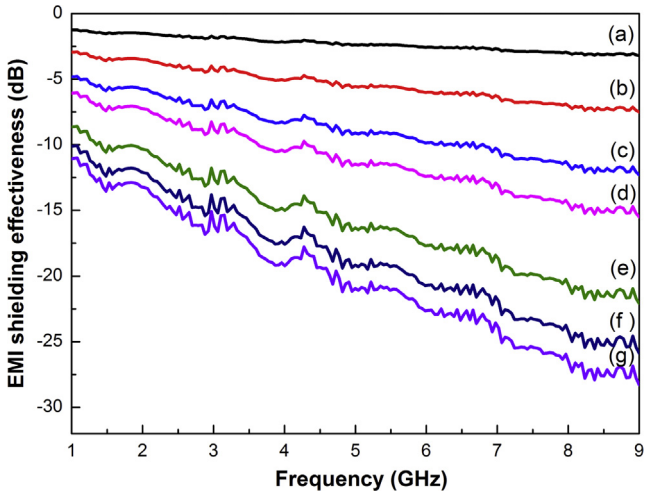

Fig. 9. EMI shielding effectiveness of NRGO/WPU composites with (a) 1 wt%, (b) 2 wt%, (c) 3 wt%, (d) 5 wt%, (e) 7 wt%, (f) 9 wt%, and (g) 12 wt% NRGO content measured in the frequency range of 1–9 GHz. (For interpretation of the references to colour in this figure legend, the reader is referred to the web version of this article.)

increasing NRGO content. With the NRGO content increasing from 1 to 12 wt%, the EMI SE of composites significantly improved. The best EMI SE of composites was 28.3 dB with 12 wt% NRGO content, which indicated that NRGO played an important role in enhancing EMI SE performances.

The total EMI SE (SE_{total}) was the sum of the reflection (SE_R), the absorption (SE_A), and internal multiple reflection (SE_M). The SE_M was generally neglected when $SE_{total} \geqslant 10$ dB, so it was generally assumed as the following equation [54–56]:

$$SE_{total} \approx SE_A + SE_R \quad (2)$$

For the NRGO/WPU composites with 12 wt% NRGO content, the values of SE_{total}, SE_A and SE_R, were 28.3 dB, 24.7 dB, and 3.6 dB, respectively at 9 GHz. It was clear that the SE_A played a vital role in the total EMI SE. Similar to previous studies, it was well understood that the conductive fillers and networks led to enhancement of EMI SE of composites [25,57,58].

3.5. Thermal stability of NRGO/WPU composites

The thermal stability of virgin WPU and NRGO/WPU composites were measured by TG and DTG under air condition. As shown in Fig. 10, the temperatures of 20% weight loss and 50% weight loss of virgin WPU appeared at 308.1 °C and 367.3 °C, respectively. Compared with the virgin WPU, the thermal decomposition temperatures of NRGO/WPU composites were tangibly improved. The 20% weight loss temperatures of NRGO/WPU composites with 3, 6, and 12 wt% NRGO were increased from 308.1 °C of virgin WPU to 320.3 °C, 337.6 °C, and 361.1 °C. In addition, the 50% weight loss temperatures of NRGO/WPU composites with 3, 6, and 12 wt% NRGO were increased from 367.3 °C of virgin WPU to 379.8 °C, 399.8 °C, and 425.8 °C. The improvement of thermal stability of NRGO/WPU composites was due to the uniform distribution of NRGO in the WPU matrix [31]. The corresponding DTG curves of virgin WPU and NRGO/WPU composites are shown in Fig. 11. The maximum degradation temperatures of NRGO/WPU composites with 3, 6, and 12 wt% NRGO were increased from 356.2 °C of virgin WPU to 361.3 °C, 372.6 °C, and 391.6 °C, respectively. The maximum degradation temperatures of composites were

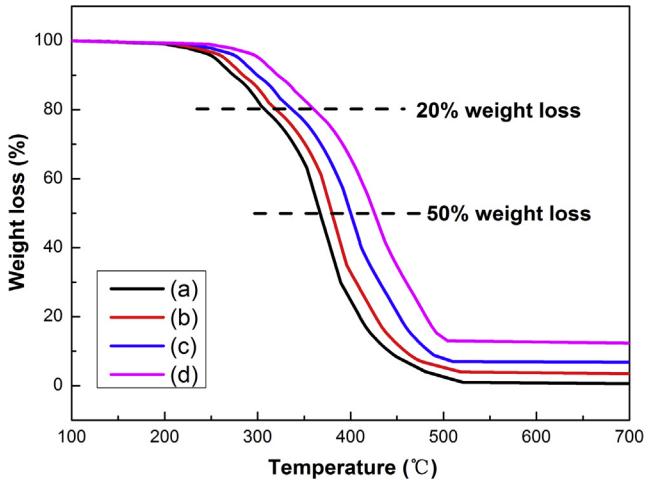

Fig. 10. TG curves of (a) virgin WPU and NRGO/WPU composites with (b) 3 wt%, (c) 6 wt%, and (d) 12 wt% NRGO content. (For interpretation of the references to colour in this figure legend, the reader is referred to the web version of this article.)

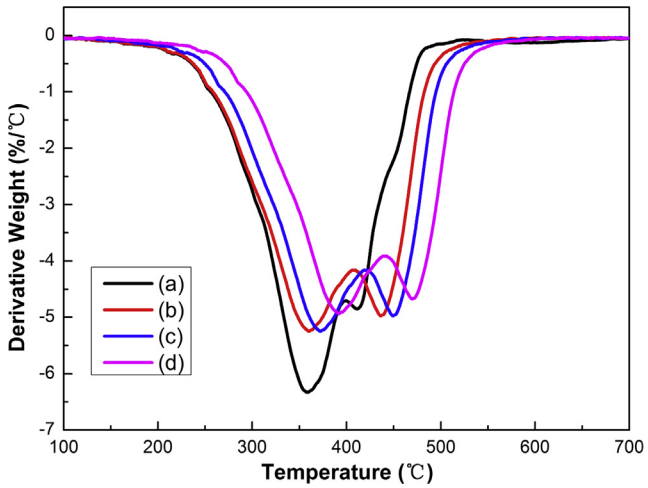

Fig. 11. DTG curves of (a) virgin WPU and NRGO/WPU composites with (b) 3 wt%, (c) 6 wt%, and (d) 12 wt% NRGO content. (For interpretation of the references to colour in this figure legend, the reader is referred to the web version of this article.)

improved with increasing NRGO content, which might be attributable to their interaction with the WPU matrix during the degradation process. Meanwhile, the NRGO/WPU composites with satisfactory thermal stability would have potential applications for the industry field.

4. Conclusion

In summary, NRGO/WPU composites were successfully prepared by the in situ chemical reduction of graphene oxide in an aqueous solution system. The uniform distribution of NRGO and its formed network structure in the WPU matrix resulted in NRGO/WPU composites with suitable electrical conductivity, EMI shielding effectiveness property, and thermal stability. The best electrical conductivity of the NRGO/WPU composites was 0.08 S/cm with 12 wt% NRGO content. Furthermore, the composites exhibited the highest EMI shielding effectiveness of 28.3 dB at 9 GHz. This preparation process provided a facile and efficient synthetic method to prepare NRGO/WPU composites, which could be used to prepare other reduced graphene oxide/polymer composites for potential applications in the EMI shielding materials.

Acknowledgment

The authors are grateful to the supports of the Natural Science Foundation of China (Grant No. 51502293), Anhui Provincial Natural Science Foundation (1408085MB39, 1508085QE112, 1508085QE110) and Youth Innovation Promotion Association, CAS (2014288, 2015268). This work is supported by "Anhui Province Key Laboratory of Environment-friendly Polymer Materials".

References

[1] Novoselov KS, Geim AK, Morozov SV, Jiang D, Zhang Y, Dubonos SV, et al. Electric field effect in atomically thin carbon films. Science 2004;306(5696):666–9.
[2] Geim AK, Novoselov KS. The rise of graphene. Nat Mater 2007;6(3):183–91.
[3] Geim AK. Graphene: status and prospects. Science 2009;324(5934):1530–4.
[4] Lee C, Wei X, Kysar JW, Hone J. Measurement of the elastic properties and intrinsic strength of monolayer graphene. Science 2008;321(5887):385–8.
[5] Stankovich S, Dikin DA, Piner RD, Kohlhaas KA, Kleinhammes A, Jia Y, et al. Synthesis of graphene-based nanosheets via chemical reduction of exfoliated graphite oxide. Carbon 2007;45(7):1558–65.
[6] Tjong SC. Graphene and its derivatives: novel materials for forming functional polymer nanocomposites. Exp Polym Lett 2012;6(6):437.
[7] Guo S, Dong S. Graphene and its derivative-based sensing materials for analytical devices. J Mater Chem 2011;21(46):18503–16.
[8] Jasuja K, Berry V. Implantation and growth of dendritic gold nanostructures on graphene derivatives: electrical property tailoring and Raman enhancement. ACS Nano 2009;3(8):2358–66.
[9] Deng D, Pan X, Yu L, Cui Y, Jiang Y, Qi J, et al. Toward N-doped graphene via solvothermal synthesis. Chem Mater 2011;23(5):1188–93.
[10] Guo B, Liu Q, Chen E, Zhu H, Fang L, Gong JR. Controllable N-doping of graphene. Nano Lett 2010;10(12):4975–80.
[11] Wang X, Li X, Zhang L, Yoon Y, Weber PK, Wang H, et al. N-doping of graphene through electrothermal reactions with ammonia. Science 2009;324(5928):768–71.
[12] Wei D, Liu Y, Wang Y, Zhang H, Huang L, Yu G. Synthesis of N-doped graphene by chemical vapor deposition and its electrical properties. Nano Lett 2009;9(5):1752–8.
[13] Qi XY, Yan D, Jiang Z, Cao YK, Yu ZZ, Yavari F, et al. Enhanced electrical conductivity in polystyrene nanocomposites at ultra-low graphene content. ACS Appl Mater Interfaces 2011;3(8):3130–3.
[14] Zheng D, Tang G, Zhang HB, Yu ZZ, Yavari F, Koratkar N, et al. In situ thermal reduction of graphene oxide for high electrical conductivity and low percolation threshold in polyamide 6 nanocomposites. Compos Sci Technol 2012;72(2):284–9.
[15] Monti M, Rallini M, Puglia D, Peponi L, Torre L, Kenny JM. Morphology and electrical properties of graphene–epoxy nanocomposites obtained by different solvent assisted processing methods. Compos A Appl Sci Manuf 2013;46(March):166–72.
[16] Grishina AD, Krivenko TV, Savel'Ev VV, Rychwalski RW, Vannikov AV. Photoelectric, nonlinear optical, and photorefractive properties of polyvinylcarbazole composites with graphene. High Energy Chem 2013;47(2):46–52.
[17] Remyamol T, John H, Gopinath P. Synthesis and nonlinear optical properties of reduced graphene oxide covalently functionalized with polyaniline. Carbon 2013;59(4):308–14.
[18] Teng CC, Ma CCM, Lu CH, Yang SY, Lee SH, Hsiao MC, et al. Thermal conductivity and structure of non-covalent functionalized graphene/epoxy composites. Carbon 2011;49(15):5107–16.
[19] Song SH, Park KH, Bo HK, Yong WC, Jun GH, Dong JL, et al. Enhanced thermal conductivity of epoxy-graphene composites by using non-oxidized graphene flakes with non-covalent functionalization. Adv Mater 2013;25(5):732–7.
[20] Achaby ME, Arrakhiz FE, Vaudreuil S, Qaiss AEK, Bousmina M, Fassi-Fehri O. Mechanical, thermal, and rheological properties of graphene-based polypropylene nanocomposites prepared by melt mixing. Polym Compos 2012;33(5):733–44.
[21] Fang M, Wang K, Lu H, Yang Y, Nutt S. Covalent polymer functionalization of graphene nanosheets and mechanical properties of composites. J Mater Chem 2009;19(19):7098–105.
[22] Zhao X, Zhang Q, Chen D, Lu P. Enhanced mechanical properties of graphene-based poly(vinyl alcohol) composites. Macromolecules 2010;43(5):2357–63.
[23] Cabrera A, Sharma P, Ayala M, Rubio-Perez L, Amézquita-Valencia M. Fabrication of exfoliated graphene-based polypropylene nanocomposites with enhanced mechanical and thermal properties. Polym Polym 2011;52(18):4001–10.
[24] Bai X, Zhai Y, Zhang Y. Green approach to prepare graphene-based composites with high microwave absorption capacity. J Phys Chem C 2011;115(23):11673–7.
[25] Ling J, Zhai W, Feng W, Shen B, Zhang J, Zheng W. Facile preparation of lightweight microcellular polyetherimide/graphene composite foams for electromagnetic interference shielding. ACS Appl Mater Interfaces 2013;5(7):2677–84.
[26] Verma M, Verma P, Dhawan SK, Choudhary V. Tailored graphene based polyurethane composites for efficient electrostatic dissipation and electromagnetic interference shielding applications. Rsc Adv 2015;5(118):97349–58.
[27] Kuilla T, Bhadra S, Yao D, Kim NH, Bose S, Lee JH. Recent advances in graphene based polymer composites. Prog Polym Sci 2010;35(11):1350–75.
[28] Kim H, Abdala AA, Macosko CW. Graphene/polymer nanocomposites. Macromolecules 2010;43(16):6515–30.
[29] Yuan FY, Zhang HB, Li X, Ma HL, Li XZ, Yu ZZ. In situ chemical reduction and functionalization of graphene oxide for electrically conductive phenol formaldehyde composites. Carbon 2014;68:653–61.
[30] Li W, Tang XZ, Zhang HB, Jiang ZG, Yu ZZ, Du XS, et al. Simultaneous surface functionalization and reduction of graphene oxide with octadecylamine for electrically conductive polystyrene composites. Carbon 2011;49(14):4724–30.
[31] Su Z, Wang H, Tian K, Xu F, Huang W, Tian X. Simultaneous reduction and surface functionalization of graphene oxide with wrinkled structure by diethylenetriamine (DETA) and their reinforcing effects in the flexible poly(2-ethylhexyl acrylate) (P2EHA) films. Compos A Appl Sci Manuf 2016;84:64–75.
[32] Hsiao ST, Ma CCM, Liao WH, Wang YS, Li SM, Huang YC, et al. Lightweight and flexible reduced graphene oxide/water-borne polyurethane composites with high electrical conductivity and excellent electromagnetic interference shielding performance. ACS Appl Mater Interfaces 2014;6(13):10667–78.
[33] Yousefi N, Gudarzi MM, Zheng QB, Lin XY, Shen X, Jia JJ, et al. Highly aligned, ultralarge-size reduced graphene oxide/polyurethane nanocomposites: mechanical properties and moisture permeability. Compos Part A – Appl Sci Manuf 2013;49:42–50.
[34] Lei L, Xia ZB, Zhang L, Zhang YH, Zhong L. Preparation and properties of amino-functional reduced graphene oxide/waterborne polyurethane hybrid emulsions. Prog Org Coat 2016;97:19–27.
[35] Hummers WS, Offeman RE. Preparation of graphitic oxide. J Am Chem Soc 1958;80(6):1339.
[36] Dreyer DR, Park S, Bielawski CW, Ruoff RS. The chemistry of graphene oxide. Chem Soc Rev 2010;39(1):228–40.
[37] Lai L, Chen L, Zhan D, Sun L, Liu J, Lim SH, et al. One-step synthesis of NH_2-graphene from in situ graphene-oxide reduction and its improved electrochemical properties. Carbon 2011;49(10):3250–7.
[38] Yang A, Li J, Zhang C, Zhang W, Ma N. One-step amine modification of graphene oxide to get a green trifunctional metal-free catalyst. Appl Surf Sci 2015;346:443–50.
[39] Jorio A. Raman spectroscopy in graphene-based systems: prototypes for nanoscience and nanometrology. Isrn Nanotechnol 2012;2012(3).
[40] Cancado LG, Jorio A, Ferreira EHM, Stavale F, Achete CA, Capaz RB, et al. Quantifying defects in graphene via Raman spectroscopy at different excitation energies. Nano Lett 2011;11(8):3190–6.
[41] Quan H, Zhang BQ, Zhao Q, Yuen RKK, Li RKY. Facile preparation and thermal degradation studies of graphite nanoplatelets (GNPs) filled thermoplastic polyurethane (TPU) nanocomposites. Compos Part A – Appl Sci Manuf 2009;40(9):1506–13.
[42] Liu J, Jeong H, Liu J, Lee K, Park JY, Ahn YH, et al. Reduction of functionalized graphite oxides by trioctylphosphine in non-polar organic solvents. Carbon 2010;48(8):2282–9.
[43] Hsiao MC, Liao SH, Yen MY, Liu PI, Pu NW, Wang CA, et al. Preparation of covalently functionalized graphene using residual oxygen-containing functional groups. ACS Appl Mater Interfaces 2010;2(11):3092–9.

[44] Kaniyoor A, Baby TT, Arockiadoss T, Rajalakshmi N, Ramaprabhu S. Wrinkled graphenes: a study on the effects of synthesis parameters on exfoliation-reduction of graphite oxide. J Phys Chem C 2011;115(36):17660–9.
[45] Wei Y, Wu J, Yin H, Shi X, Yang R, Dresselhaus M. The nature of strength enhancement and weakening by pentagon-heptagon defects in graphene. Nat Mater 2012;11(9):759–63.
[46] Chen Y, Wang Y, Zhang H-B, Li X, Gui C-X, Yu Z-Z. Enhanced electromagnetic interference shielding efficiency of polystyrene/graphene composites with magnetic Fe_3O_4 nanoparticles. Carbon 2015;82:67–76.
[47] Zhang SD, Li YF, Peng LQ, Li QF, Chen SL, Hou K. Synthesis and characterization of novel waterborne polyurethane nanocomposites with magnetic and electrical properties. Compos Part A – Appl Sci Manuf 2013;55:94–101.
[48] Tang XZ, Mu C, Zhu W, Yan X, Hu X, Yang J. Flexible polyurethane composites prepared by incorporation of polyethylenimine-modified slightly reduced graphene oxide. Carbon 2015;98:432–40.
[49] Kim F, Cote LJ, Huang J. Graphene oxide: surface activity and two-dimensional assembly. Adv Mater 2010;22(17):1954–8.
[50] Yousefi N, Gudarzi MM, Zheng Q, Aboutalebi SH, Sharif F, Kim JK. Self-alignment and high electrical conductivity of ultralarge graphene oxide–polyurethane nanocomposites. J Mater Chem 2012;22(25):12709–17.
[51] Kim J, Cote LJ, Kim F, Yuan W, Shull KR, Huang J. Graphene oxide sheets at interfaces. J Am Chem Soc 2010;132(23):8180–6.
[52] Wu Z, Wang H, Xue M, Tian X, Zhou H, Ye X, et al. Preparation of carbon nanotubes/waterborne polyurethane composites with the emulsion particles assisted dispersion of carbon nanotubes. Compos Sci Technol 2015;114:50–6.
[53] Kirkpatrick S. Percolation and conduction. Rev Mod Phys 1973;45(4):574–88.
[54] Chen Z, Xu C, Ma C, Ren W, Cheng H-M. Lightweight and flexible graphene foam composites for high-performance electromagnetic interference shielding. Adv Mater 2013;25(9):1296–300.
[55] Yuan B, Yu L, Sheng L, An K, Zhao X. Comparison of electromagnetic interference shielding properties between single-wall carbon nanotube and graphene sheet/polyaniline composites. J Phys D Appl Phys 2012;45(23):6705–11.
[56] Kim HR, Kim BS, Kim IS. Fabrication and EMI shielding effectiveness of Ag-decorated highly porous poly(vinyl alcohol)/Fe_2O_3 nanofibrous composites. Mater Chem Phys 2012;135(2–3):1024–9.
[57] Mural PKS, Pawar SP, Jayanthi S, Madras G, Sood AK, Bose S. Engineering nanostructures by decorating magnetic nanoparticles onto graphene oxide sheets to shield electromagnetic radiations. ACS Appl Mater Interfaces 2015;7(30):16266–78.
[58] Yan DX, Ren PG, Pang H, Fu Q, Yang MB, Li ZM. Efficient electromagnetic interference shielding of lightweight graphene/polystyrene composite. J Mater Chem 2012;22(36):18772–4.